

Autonomous stabilization with programmable stabilized state

Received: 20 February 2024

Accepted: 2 August 2024

Published online: 14 August 2024

 Check for updates

Ziqian Li^{1,2,3}✉, Tanay Roy^{1,2,4}, Yao Lu^{1,2,4}, Eliot Kapit⁵ & David I. Schuster^{1,2,3,6}

Reservoir engineering is a powerful technique to autonomously stabilize a quantum state. Traditional schemes involving multi-body states typically function for discrete entangled states. In this work, we enhance the stabilization capability to a continuous manifold of states with programmable stabilized state selection using multiple continuous tuning parameters. We experimentally achieve 84.6% and 82.5% stabilization fidelity for the odd and even-parity Bell states as two special points in the manifold. We also perform fast dissipative switching between these opposite parity states within 1.8 μ s and 0.9 μ s by sequentially applying different stabilization drives. Our result is a precursor for new reservoir engineering-based error correction schemes.

Entanglement is one major resource any quantum protocol utilizes to achieve quantum advantage^{1,2}. Generally, the entanglement is created by unitary operations, where dissipation is considered detrimental and should be maximally avoided. Inspired by laser cooling, an alternative approach is to use tailored dissipation for stabilizing entanglement. By coupling the qubit system to some cold reservoirs, one can engineer the Hamiltonian such that the population will flow directionally to the stabilized point in the Hilbert space, and extra entropy is autonomously dumped into the cold reservoir during the process. This provides an extra route to state preparation. In a multiqubit-reservoir coupled system, dissipation engineering can enhance the capabilities of quantum simulation, as predicting the final state of a driven dissipative quantum system is more complex than its unitary counterpart³ when all local qubit and reservoir interactions are simultaneously turned on. Dissipation stabilization also inspires autonomous quantum error correction codes (AQEC)^{4–9} that achieve hardware efficiency in the experiment.

Stabilization has been theoretically proposed and experimentally realized in different platforms, such as superconducting qubits^{10–17} and trapped ions^{18,19}, focusing on stabilizing a single special state per device, such as even or odd parity Bell states. Unlike universal quantum state preparation through unitary gate decomposition, dissipative stabilization requires individual Hamiltonian engineering for each stabilized state through different drive combinations or hardware.

This makes the tunable dissipative stabilization a challenging task. A generalized scheme that allows one to programmatically choose stabilized states from a large class of states per device will expand the toolbox for state preparation. For instance, the ability to choose an arbitrary stabilized state can be used for the implementation of density matrix exponentiation^{20,21} by enabling an efficient reset of the input density matrix.

In this work, we realize an autonomous stabilization protocol with superconducting circuits that allows selection from a broad class of states, including the maximally entangled states. We use microwave-only drives with tunable parameters such as drive detunings and strengths that allow fast programmable switching between Bell states of different parities. The system is based on a two-transmon inductive coupler design^{8,17,22,23} that allows fast parametric interactions between qubits without significantly compromising their coherence. The readout resonators are also used as cold reservoirs, eliminating the requirement for extra components. We perform stabilization spectroscopy and demonstrate a fidelity over 78% for all stabilized states. For odd and even parity Bell pairs, we measured 84.6% and 82.5% stabilization fidelity and a stabilization time of 1.8 μ s and 0.9 μ s respectively. The current stabilization protocol cannot realize AQEC, and a larger code distance between logical states is necessary^{8,9} for demonstrating quantum error correction. The structure of the paper is as follows. First, we explain the Hamiltonian construction of the

¹James Franck Institute, University of Chicago, Chicago, IL, USA. ²Department of Physics, University of Chicago, Chicago, IL, USA. ³Department of Applied Physics, Stanford University, Stanford, CA, USA. ⁴Superconducting Quantum Materials and Systems Center, Fermi National Accelerator Laboratory (FNAL), Batavia, IL, USA. ⁵Department of Physics, Colorado School of Mines, Golden, CO, USA. ⁶Pritzker School of Molecular Engineering, University of Chicago, Chicago, IL, USA. ✉e-mail: zqianli@uchicago.edu

stabilization protocol. Then we discuss the experimental measurement of individual stabilized state and demonstrate a dissipative switch of Bell state parity.

Results

Stabilization theory

We consider a system of two coupled qubit-resonator pairs $\{Q_1, Q_2\}$ and $\{R_1, R_2\}$. The lossy resonators serve as both cold baths and dispersive readouts for the qubits. We label the ground and the first excited states of the qubits $Q_{1/2}$ as $|g\rangle$ and $|e\rangle$, and of the resonators $R_{1/2}$ as $|0\rangle$ and $|1\rangle$, with the full system state being represented as $|Q_1 Q_2 R_1 R_2\rangle$. The system Hamiltonian $H_{\text{sys}} = H_{QQ} + H_{QR1} + H_{QR2}$ includes the dominant two-qubit interaction H_{QQ} and qubit-resonator interactions $H_{QRj}, j = 1, 2$ acting as perturbations. We label the four eigenstates of H_{QQ} as $\{|A\rangle, |B\rangle, |C\rangle, |D\rangle\}$ with eigenenergies $\{E_A < E_B \leq E_C \leq E_D\}$ so that $|A\rangle$ is the target state to stabilize. Our stabilization scheme involves engineering a one-way flow of population to $|A\rangle$ connecting all intermediate eigenstates of the system.

We now derive the energy matching requirements for an efficient stabilization protocol in our two-qubit-two-resonator system depicted in Fig. 1a. We control the form of the target stabilized state $|A\rangle$ by choosing different two-qubit interaction strengths and detunings that control H_{QQ} . We change the resonator photon energy in the rotating frame by detuning the QR interactions. The dynamics of H_{sys} are captured by considering the following set of eigenstates: $\{|A\rangle, |B\rangle, |C\rangle, |D\rangle\} \otimes \{|00\rangle, |10\rangle, |01\rangle\}$. We neglect the resonator state $|11\rangle$ as the probability of simultaneous population in both resonators $\{R_1, R_2\}$ is extremely low when resonator decay rate κ is much larger than the qubit decay rate γ (assumed identical). The central column in Fig. 1(a) shows the eigenstates of H_{QQ} with no photons in the resonators. The left column represents the same states with one photon in the left (R_1) resonator and similarly for the right column is associated with the second resonator (R_2). We engineer the photon energies in R_1 and R_2 to be $E_B - E_A$ and $E_C - E_A$ respectively through tuning the QR interactions H_{QRj} . This condition puts two transitions $|A01\rangle \leftrightarrow |C00\rangle$ and $|A10\rangle \leftrightarrow |B00\rangle$ on resonance, shown in Fig. 1a. If $\langle A01|H_{QR1}|C00\rangle$ and $\langle A10|H_{QR2}|B00\rangle$ are non-zero, two on-resonance oscillations between $|C00\rangle$, $|A01\rangle$ and between $|A10\rangle$, $|B00\rangle$ will be created. Since both resonators are lossy, the oscillation will quickly damp to $|A00\rangle$. To complete the downward stabilization path, we need to also connect $|D00\rangle$ into the flow. We further require that the following terms are non-zero so that the transfer path is not blocked: $\langle B01|H_{QR1}|D00\rangle$, $\langle C10|H_{QR2}|D00\rangle$. If all four interaction strengths (shown in green double-headed arrows in Fig. 1a) are dominant over the qubit decay rate, populations in $|B\rangle$, $|C\rangle$, and $|D\rangle$ will flow to $|A\rangle$. From Fermi's golden rule, the interaction strength between two states is quadratically suppressed by their energy gap and maximized when on-resonance²⁴. This imposes a simple energy-matching requirement for efficient stabilization: $E_D + E_A = E_B + E_C$. Energy degeneracy within $\{|B\rangle, |C\rangle, |D\rangle\}$ will not affect the stabilization scheme, because it will not block the dissipative flow to $|A00\rangle$ in Fig. 1a.

As an explicit demonstration, we first stabilize a continuous set of entangled states $|\Psi_\theta\rangle = \sin(\theta/2)|gg\rangle - \cos(\theta/2)|ee\rangle$, illustrated in Fig. 1b. Here, θ can be regarded as a “blending angle” between the two even parity states $|gg\rangle$ and $|ee\rangle$. We introduce three sideband²⁵ transitions into the system: qubit-qubit (QQ) blue sideband $|gg\rangle \leftrightarrow |ee\rangle$ with rate Ω and two qubit-resonator (QR) blue sidebands $|g0\rangle \leftrightarrow |e1\rangle$ between Q_j and R_j with rate W_j . In this context, ‘sideband’ refers to a two-photon process where either a single photon is exchanged at the frequency difference (known as the red sideband) or two photons are simultaneously driven at the frequency sum (referred to as the blue sideband). To ensure that H_{QRj} act as perturbations over H_{QQ} , we adjust the drive strengths to satisfy $\Omega \gg W_j$. We further detune the QQ, QRI, and QR2 blue sideband by δ , $(\Delta - \delta)/2$, and $(\Delta + \delta)/2$ in frequencies, with $\Delta = \sqrt{\Omega^2 + \delta^2}$. The detuning δ determines the blending angle

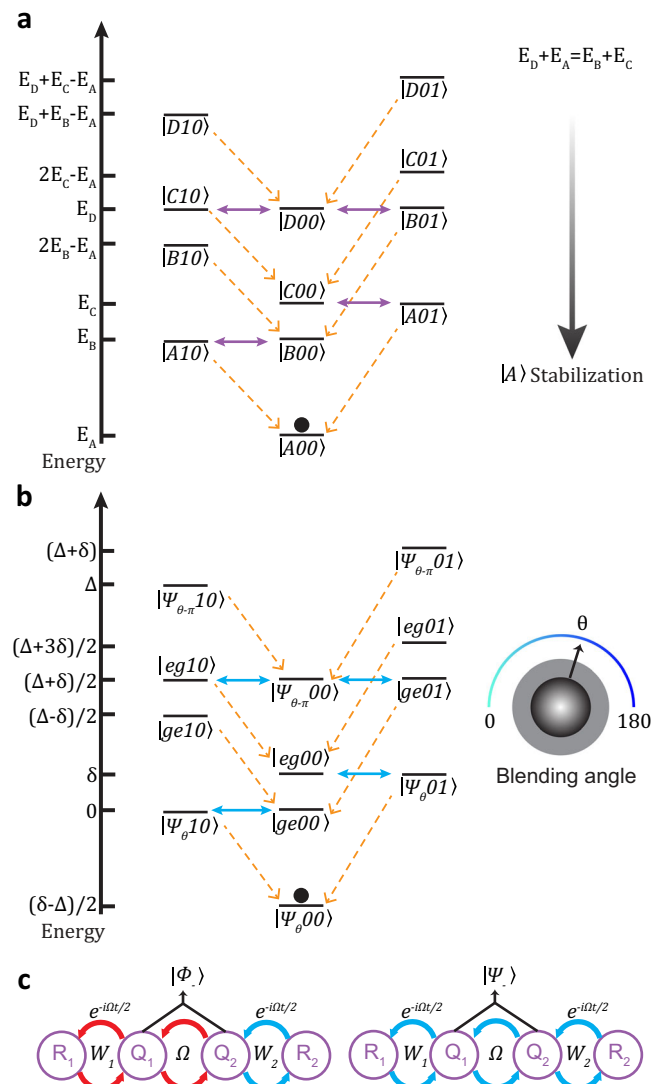


Fig. 1 | Programmable stabilization protocol. **a** General stabilization scheme. Two qubits' eigenstates $\{|A\rangle, |B\rangle, |C\rangle, |D\rangle\}$ are plotted in the energy level diagram. When the energy relation $E_D + E_A = E_B + E_C$ is satisfied, $|A\rangle$ is stabilized. Qubit-resonator interactions and resonator photon decay rate κ are shown in blue and orange arrows. Qubit decay rate γ is assumed slowest and not plotted. **b** Stabilization of entangled states $|\Psi_\theta\rangle = \sin(\theta/2)|gg\rangle - \cos(\theta/2)|ee\rangle$ or $|\Phi_\theta\rangle = \sin(\theta/2)|ge\rangle - \cos(\theta/2)|eg\rangle$. **c** A special case of **b** that stabilizes the odd and even parity bell states $|\Phi_-\rangle$ and $|\Psi_-\rangle$. Circulating arrows are color-coded to represent red (exchange-like) and blue (two-photon-pumping) sidebands respectively. The QQ and QR sideband rates are separate Ω and W_j , and the QR sideband is detuned in frequency by $\Omega/2$.

$\theta = \tan^{-1}(\frac{\delta + \Delta}{\Omega})$ with a range of $[0, \frac{\pi}{2}]$. In the presence of these three drives, the rotating frame Hamiltonian H_{sys} is

$$H_{\text{sys}} = \frac{\Omega}{2} (a_{q1} a_{q2} + h.c.) + \delta a_{q1}^\dagger a_{q1} + \frac{W_1}{2} (a_{q1} a_{r1} + h.c.) + \frac{W_2}{2} (a_{q2} a_{r2} + h.c.) + \frac{\Delta + \delta}{2} a_{r1}^\dagger a_{r1} + \frac{\Delta - \delta}{2} a_{r2}^\dagger a_{r2}. \quad (1)$$

Here a_{qj} and a_{rj} are separately the j -th qubit's and resonator's annihilation operator. Anharmonicity α is omitted from Equation (1) by treating both transmons as two-level systems. The presence of anharmonicity effectively suppresses the higher energy levels'

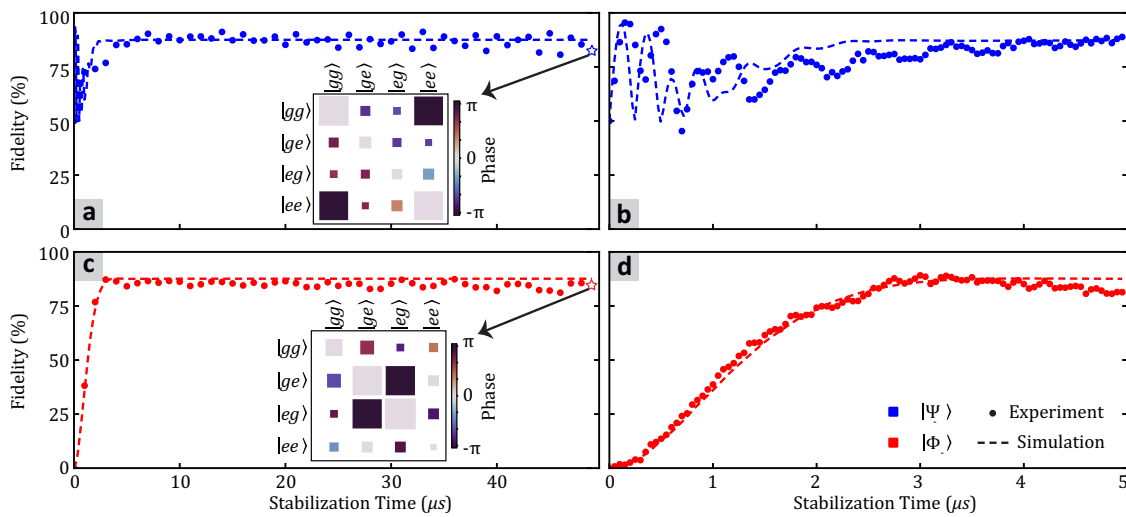


Fig. 2 | Experimental stabilization of different Bell states. Experimental demonstration of $|\Psi_-\rangle$ (a, b) and $|\Phi_-\rangle$ (c, d) stabilization with the initial state $|gg\rangle$. Two-qubit state tomography is performed at each time point, and the reconstructed density matrix is used to calculate the target state fidelity. The density matrices reconstructed with 5000 single shot measurements at $49\ \mu\text{s}$ are plotted.

Lab frame simulation results are shown in dash lines, which matched well in both short and long time scales. Parameters used in simulation: $\{\Omega, W_1, W_2, \Gamma_1, \Gamma_2\}/2\pi = \{2.0, 0.47, 0.47, 0.33, 0.43\}$ MHz for $|\Psi_-\rangle$ and $\{3.0, 0.36, 0.36, 0.33, 0.43\}$ MHz for $|\Phi_-\rangle$. Qubit coherence time is chosen as $\{T_1^{q1}, T_1^{q2}, T_\phi^{q1}, T_\phi^{q2}\} = \{25, 12, 25, 25\}$ μs . Error bars (one standard deviation) are smaller than the marker size²⁷.

population in either transmon. Under the combined conditions $\Omega \gg W_j \sim \kappa \gg \gamma$ and $W_j = W$, the eigenstates with zero resonator photons are $(|\Psi_\theta 00\rangle, |ge00\rangle, |leg00\rangle, |\Psi_{\theta-\pi} 00\rangle)$, with corresponding eigenenergies $\{(\delta - \Delta)/2, 0, \delta, (\delta + \Delta)/2\}$. Assuming the lossy resonator has a Lorentzian energy spectrum, the two-step refilling rate Γ_t from $|leg00\rangle$ to $|\Psi_\theta 00\rangle$ ($|leg00\rangle \leftrightarrow |\Psi_\theta 01\rangle, |\Psi_\theta 01\rangle \rightarrow |\Psi_\theta 00\rangle$) is²⁴

$$\Gamma_t = \frac{W^2 \cos^2(\theta/2) \kappa}{\kappa^2 + W^2 \cos^2(\theta/2)}. \quad (2)$$

The other two-step transitions $|ge00\rangle \rightarrow |\Psi_\theta 00\rangle$, $|\Psi_{\theta-\pi} 00\rangle \rightarrow |ge00\rangle$, and $|\Psi_{\theta-\pi} 00\rangle \rightarrow |leg00\rangle$ also have the same rate. Therefore, the steady-state fidelity \mathcal{F}_∞ for $|\Psi_\theta 00\rangle$ is (ignoring all off-resonant transitions, see Supplementary Note 2 for detail)

$$\mathcal{F}_\infty = \left(\frac{\Gamma_t + \gamma \sin^2(\theta/2)}{\Gamma_t + \gamma} \right)^2. \quad (3)$$

Similarly, we can stabilize another set of entangled states with odd parity $|\Phi_\theta\rangle = \sin(\theta/2)|ge\rangle - \cos(\theta/2)|leg\rangle$. We introduce three sideband interactions: QQ red $|eg\rangle \leftrightarrow |ge\rangle$, QRI red $|e0\rangle \leftrightarrow |g1\rangle$, and QR2 blue $|g0\rangle \leftrightarrow |e1\rangle$ with rates $\{\Omega, W_3, W_4\}$ and frequency detunings $\{\delta, (\Delta + \delta)/2, (\Delta - \delta)/2\}$ respectively. Under this condition, four resonant interactions will appear: $|gg00\rangle \leftrightarrow |\Phi_\theta 01\rangle$, $|ee00\rangle \leftrightarrow |\Phi_\theta 10\rangle$, $|ee01\rangle \leftrightarrow |\Phi_{\theta-\pi} 00\rangle$, and $|gg10\rangle \leftrightarrow |\Phi_{\theta-\pi} 00\rangle$. The detuning similarly sets the blending angle $\theta = \arctan(\frac{\delta + \Delta}{\Omega})$.

With the above construction, we create a stabilization protocol that can freely tune the blending angles. As a special case, when QQ sideband detuning $\delta = 0$, the blending angle for both cases is $\theta = \frac{\pi}{2}$, which corresponds to the odd and even parity Bell states $|\Phi_-\rangle = (|ge\rangle - |leg\rangle)/\sqrt{2}$ and $|\Psi_-\rangle = (|gg\rangle - |ee\rangle)/\sqrt{2}$, shown in Fig. 1c.

In fact, this stabilization protocol can be generalized to stabilize an even larger group of states, including both entangled and product states, as long as the energy matching requirement $E_D + E_A = E_B + E_C$ is satisfied when engineering H_{QQ} . The following is a list of tunable parameters to engineer H_{QQ} : QQ sideband strength Ω , QQ sideband detunings δ , single qubit Rabi drive strength, and single qubit Rabi

drive detunings. Corresponding stabilized state $|A\rangle$ is determined from H_{QQ} . Details about the stabilizable manifold are discussed in Supplementary Note 4.

Experimental results

We perform the stabilization experiment in a system with two transmons capacitively coupled to two lossy resonators (See Supplementary Note 1). Two transmons are inductively coupled through a SQUID loop. All QQ sidebands and QR red sidebands are realized through modulating the SQUID flux at corresponding transition frequencies. QR blue sidebands are achieved by sending a charge drive to the transmon at half the transition frequencies. The experimentally measured qubit coherence are $T_1 = 24.3\ \mu\text{s}$ ($9.1\ \mu\text{s}$), $T_{\text{Ram}} = 15.2\ \mu\text{s}$ ($9.8\ \mu\text{s}$), $T_{\text{echo}} = 24.6\ \mu\text{s}$ ($14.3\ \mu\text{s}$) for Q_1 (Q_2), and the measured resonator decay rate $\kappa/2\pi$ are $\{0.33, 0.43\}$ MHz for R_1 and R_2 respectively.

Figure 2 shows the time evolution of state fidelity for the odd and even parity Bell state stabilization. To stabilize $|\Psi_-\rangle$, a $\Omega = 2\pi \times 2.0$ MHz QQ blue sideband, $W_1 = W_2 = 2\pi \times 0.47$ MHz QR blue sidebands are simultaneously applied to the system. Both QR sidebands are detuned by $\Omega/2 = 2\pi \times 1.0$ MHz in frequency to implement the stabilization scheme depicted in Fig. 1(c). For each stabilization experiment, we reconstruct the system density matrix through two-qubit state tomography using 5000 repetitions of 9 different pre-rotations. The stabilization fidelity measured at $49\ \mu\text{s}$ (much longer than single qubit T_1 and T_{Ram}) is 82.5%. To stabilize $|\Phi_-\rangle$, a $\Omega = 2\pi \times 3.0$ MHz QQ red sideband, $W_1 = W_2 = 2\pi \times 0.36$ MHz QRI red and QR2 blue sidebands are simultaneously applied to the system, with both QR sidebands detuned by $\Omega/2 = 2\pi \times 1.5$ MHz. The stabilization fidelity measured at $49\ \mu\text{s}$ is 84.6%. The two-qubit state tomography data at $49\ \mu\text{s}$ after ZZ coupling correction²⁶ are shown for both stabilization cases. Fidelities are calculated as $F = (\text{tr} \sqrt{\sqrt{\rho} \sigma \sqrt{\rho}})^2$, where σ is the target state and ρ is the tomography reconstructed density matrix. Error bars (one standard deviation) for all expectation values calculated from the Maximum Likelihood Estimation (MLE) reconstructed density matrix use the Tomographer package²⁷.

Next, we introduce QQ sideband detunings δ and stabilize more general entangled states $|\Psi_\theta\rangle$ and $|\Phi_\theta\rangle$. We choose the same sideband strengths $\{\Omega, W_1, W_2\}/2\pi = \{2.0, 0.47, 0.47\}/\{3.0, 0.36, 0.36\}$ MHz for

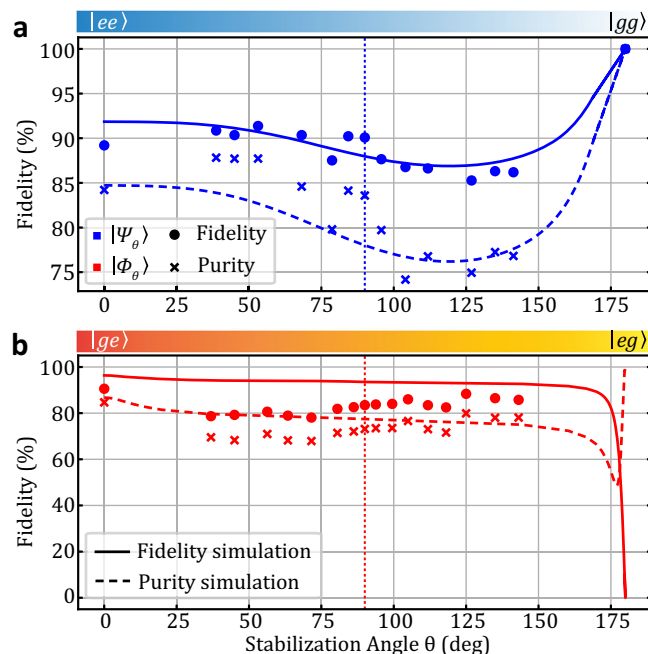


Fig. 3 | Spectroscopy of universal Bell-state stabilization. $|\Psi_\theta\rangle$ **a** and $|\Phi_\theta\rangle$ **b** are separately stabilized with a measured fidelity above 78% among different blending angle θ . The fidelities are measured after 40 μs of stabilization. For stabilizing $|gg\rangle$, no external drives are applied. For $|\Phi_\theta\rangle$ case, the fidelity dropped to 0 near $\theta = \pi$. The dotted lines indicate simulated fidelities for the odd and even parity Bell state stabilization. All parameters used in the simulation are the same as in Fig. 2. Error bars (one standard deviation) are smaller than the marker size²⁷.

$|\Psi_\theta\rangle(|\Phi_\theta\rangle)$ case) and detune QR sideband frequencies accordingly to maximize the stabilization fidelity measured at 40 μs . The experimentally measured state fidelity and state purity as a function of θ are shown in Fig. 3. Under the current QR sideband color combination, $|\Phi_\theta\rangle$ fails to stabilize near $\theta = 180^\circ$. This is because the interaction strength $\langle gg00|H_{\text{sys}}|\Phi_\theta 01\rangle$ and $\langle ee00|H_{\text{sys}}|\Phi_\theta 10\rangle$ are close to 0. Swapping QR1 and QR2 sidebands' color and detuning performs a transformation $\theta \rightarrow \theta - \pi$ in the stabilized state. This ensures a high stabilization fidelity for arbitrary stabilization angles. Details about changing sideband colors and detunings to ensure high fidelity are presented in Supplementary Note 6.

The flexibility in our schemes and easy access to different sidebands in our device allow a further demonstration—fast dissipative switching between stabilized states. Here, we implement such an operation that can flip the parity of the stabilized Bell pair by changing sideband combinations, shown in Fig. 1. To quantify the stabilized parity, we measure the system's density matrix ρ and define the parity signature as $2(|\langle ee|\rho|gg\rangle| - |\langle ge|\rho|eg\rangle|)$ describing the difference in relevant coherence parameters. The results are shown in Fig. 4. The scaling factor is chosen such that the ideal even and odd Bell pairs have parity signatures of ± 1 . Starting from the ground state $|Q_1 Q_2\rangle = |gg\rangle$, the stabilized state is set to even parity Bell pair $(|gg\rangle - |ee\rangle)/\sqrt{2}$, and we switch the parity every 20 μs . At 20 μs , the stabilized state is switched to odd parity Bell pair $(|ge\rangle - |eg\rangle)/\sqrt{2}$, and stabilization happens quickly with a time constant $\tau_r = 1.8 \mu\text{s}$. At 40 μs , the switching from odd to even parity results in a faster stabilization with $\tau_b = 0.91 \mu\text{s}$. The switching at 60 μs to odd Bell state shows a similar τ_b of 2.20 μs . We leave the stabilization drives turned on for another 25 μs to prove that the performance is not degraded after a few switching operations.

Further improvement of the stabilized state's fidelity is possible by reducing the transition ratio $\frac{\gamma}{\Gamma_r}$ (from Eq. (3)) and increasing QQ sideband rate Ω for a larger energy gap. Increasing qubit dephasing

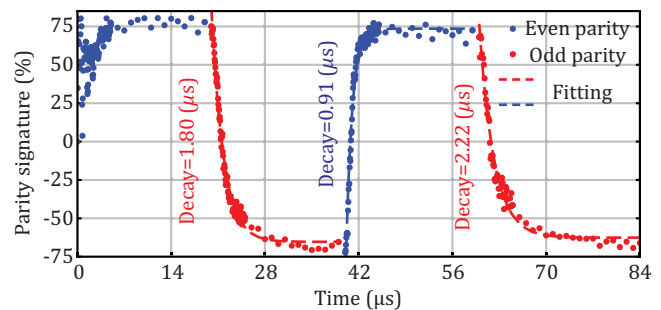


Fig. 4 | Dissipative switching of Bell state parity. The initial state is $|gg\rangle$, and the switch status is set to even parity between $[0 \mu\text{s}, 20 \mu\text{s}]$ and $[40 \mu\text{s}, 60 \mu\text{s}]$, and to odd parity between $[20 \mu\text{s}, 40 \mu\text{s}]$ and $[60 \mu\text{s}, 85 \mu\text{s}]$. Each experimental point is measured with the two-qubit state tomography. Stabilization time is calculated by fitting the parity signature to exponential decay after each switching event.

time also improves stabilization fidelity (discussed in the Supplementary Note 3). To speed up the stabilization, i.e., reduce time constants, we need to increase the refilling rate Γ_r . Since QR sideband rate W is bounded by the QQ sideband rate Ω to ensure the validity of the perturbative approximation, given a fixed W , Γ_r is maximized when the resonator decay rate $\kappa = W \cos(\theta/2)$. For the even and odd parity Bell states, further increase in both resonators' κ compared to our current parameters would thus be beneficial. More details about stabilization robustness are discussed in Supplementary Note 3. To stabilize a more general set of states shown in Supplementary Note 4, longer qubit coherence is needed to improve the experimental resolution between different stabilized states in this manifold and is a subject of future work. Details about stabilization infidelities are discussed in Methods.

Discussion

In conclusion, we demonstrate a two-qubit programmable stabilization scheme that can autonomously stabilize a continuous set of entangled states. We develop an inductively coupled two-qubit device that provides access to both QQ and QR sideband interactions required. The stabilization fidelity among all stabilization angles is above 78%, specifically, we achieved high Bell pair stabilization fidelity (84.6% for the odd parity and 82.5% for the even parity) as two special points. We further demonstrate a parity switching capability between the Bell pairs with fast stabilization time constants ($< 2 \mu\text{s}$). To realize AQEC, the refilling rate from the error state to the logical state should be much faster than the error rate. The fast switching rate between different stabilized states, which is over an order of magnitude larger than the transmons' decay and dephasing rate, is sufficient for AQEC. We believe such freedom in choosing stabilized states will inspire generalization to autonomous stabilization of larger systems, large-scale many-body entanglement³, remote entanglement²⁸, and density matrix exponentiation^{20,21}. While the current stabilization protocol cannot stabilize a logical manifold, it is possible to generalize this to new AQEC logical codewords by incorporating higher transmon levels⁸ or by utilizing additional transmons in future developments.

Methods

Experimental error analysis

To accurately simulate the real system, we sequentially introduce several error channels. After each addition, we calculate its contribution to infidelity by measuring the difference in the steady-state fidelity. We use the states $|\Phi_-\rangle$ and $|\Psi_-\rangle$ as examples, with results detailed in Table 1.

Initially, in an ideal case, decoherence-free simulations are conducted within a Hamiltonian of dimension $2 \times 2 \times 2 \times 2$ (two levels per

Table 1 | Infidelity channels for odd and even parity Bell states stabilization

Stabilized state infidelity	$ \Phi_-\rangle$	$ \Psi_-\rangle$
Ideal implementation	1.71%	4.98%
Transmon T_1	7.56%	5.25%
Transmon dephasing	3.14%	2.21%
$ f\rangle$ state leakage	$\sim 0.1\%$	$\sim 0.1\%$
ZZ interactions	0.85%	0.98%
Thermal excitation ¹	$\sim 2.0\%$	$\sim 2.0\%$
QR frequency mismatch ¹	<0.18%	<0.57%
QQ frequency mismatch ¹	<0.1%	<0.1%
Total predicted fidelity	$\sim 15.64\%$	$\sim 16.19\%$
Experimental infidelity	15.4%	17.5%

¹ The transmon excitation rate is approximately 0.9 ms, as inferred from the residual infidelities observed in the experiments.

¹ Frequency mismatch are assumed to be at most 20 kHz.

resonator), resulting in infidelities of 1.71% and 4.98% respectively. Subsequently, transmon T_1 and T_ϕ are incorporated into the system, revealing that transmon decoherence accounts for the majority of the stabilization infidelity observed in experiments. A higher transmon level is then added, extending the Hamiltonian to a dimension of $3 \times 3 \times 2 \times 2$. The contribution of transmon ZZ coupling to the stabilization infidelities is found to be less than 1%. Other error channels contribute minimally, such as leakage to the $|f\rangle$ state and inaccuracies in sideband frequency calibration. The discrepancy between the theoretically predicted and experimentally measured state fidelities is primarily attributed to the thermal excitation rate in the transmons when all sidebands are active. An excitation rate of 0.9 ms in both transmons sufficiently explains these deviations in the simulation.

Tomography error bar

Error bars (one standard deviation) for all expectation values calculated from the Maximum Likelihood Estimation(MLE) reconstructed density matrix use the Tomographer package²⁷.

Data availability

Source data are provided with the paper²⁹. All data used within this paper are available from the corresponding author upon request.

Code availability

Simulation codes are provided with the paper²⁹. All other codes used within this paper are available from the corresponding author upon request.

References

1. Arute, F. et al. Quantum supremacy using a programmable superconducting processor. *Nature* **574**, 505 (2019).
2. Wu, Y. et al. Strong quantum computational advantage using a superconducting quantum processor. *Phys. Rev. Lett.* **127**, 180501 (2021).
3. Kapit, E., Roushan, P., Neill, C., Boixo, S. & Smelyanskiy, V. Entanglement and complexity of interacting qubits subject to asymmetric noise. *Phys. Rev. Res.* **2**, 043042 (2020).
4. Verstraete, F., Wolf, M. M. & Ignacio Cirac, J. Quantum computation and quantum-state engineering driven by dissipation. *Nat. Phys.* **5**, 633 (2009).
5. Kapit, E. Hardware-efficient and fully autonomous quantum error correction in superconducting circuits. *Phys. Rev. Lett.* **116**, 150501 (2016).
6. Ma, Y. et al. Error-transparent operations on a logical qubit protected by quantum error correction. *Nat. Phys.* **16**, 827 (2020).
7. Gertler, J. M. et al. Protecting a bosonic qubit with autonomous quantum error correction. *Nature* **590**, 243 (2021).
8. Li, Z. et al. Autonomous error correction of a single logical qubit using two transmons. *Nat. Commun.* **15**, 1681 (2024).
9. Li, Z., Roy, T., Pérez, D. R., Schuster, D. I. & Kapit, E. Hardware-efficient autonomous error correction with linear couplers in superconducting circuits. *Phys. Rev. Res.* **6**, 013171 (2024).
10. Shankar, S. et al. Autonomously stabilized entanglement between two superconducting quantum bits. *Nature* **504**, 419 (2013).
11. Kimchi-Schwartz, M. E. et al. Stabilizing entanglement via symmetry-selective bath engineering in superconducting qubits. *Phys. Rev. Lett.* **116**, 240503 (2016).
12. Lu, Y. et al. Universal stabilization of a parametrically coupled qubit. *Phys. Rev. Lett.* **119**, 150502 (2017).
13. Huang, Z., Lu, Y., Kapit, E., Schuster, D. I. & Koch, J. Universal stabilization of single-qubit states using a tunable coupler. *Phys. Rev. A* **97**, 062345 (2018).
14. Andersen, C. K. et al. Entanglement stabilization using ancilla-based parity detection and real-time feedback in superconducting circuits. *npj Quantum Information* **5**, 69 (2019).
15. Ma, S.-I., Li, X.-k., Liu, X.-y., Xie, J.-k. & Li, F.-l. Stabilizing bell states of two separated superconducting qubits via quantum reservoir engineering. *Phys. Rev. A* **99**, 042336 (2019).
16. Bultink, C. C. et al. Protecting quantum entanglement from leakage and qubit errors via repetitive parity measurements. *Sci. Adv.* **6**, eaay3050 (2020).
17. Brown, T. et al. Trade off-free entanglement stabilization in a superconducting qutrit-qubit system. *Nat. Commun.* **13**, 3994 (2022).
18. Lin, Y. et al. Dissipative production of a maximally entangled steady state of two quantum bits. *Nature* **504**, 415 (2013).
19. Cole, D. C. et al. Resource-efficient dissipative entanglement of two trapped-ion qubits. *Phys. Rev. Lett.* **128**, 080502 (2022).
20. Lloyd, S., Mohseni, M. & Rebentrost, P. Quantum principal component analysis. *Nat. Phys.* **10**, 631 (2014).
21. Kjaergaard, M. et al. Demonstration of density matrix exponentiation using a superconducting quantum processor. *Phys. Rev. X* **12**, 011005 (2022).
22. Lu, Y. Parametric control of flux-tunable superconducting circuits <https://doi.org/10.6082/uchicago.1973> (2019)
23. Roy, T., Li, Z., Kapit, E. & Schuster, D. Two-qutrit quantum algorithms on a programmable superconducting processor. *Phys. Rev. Appl.* **19**, 064024 (2023).
24. Kapit, E., Hafezi, M. & Simon, S. H. Induced self-stabilization in fractional quantum hall states of light. *Phys. Rev. X* **4**, 031039 (2014).
25. Wallraff, A. et al. Sideband transitions and two-tone spectroscopy of a superconducting qubit strongly coupled to an on-chip cavity. *Phys. Rev. Lett.* **99**, 050501 (2007).
26. Roy, T., Li, Z., Kapit, E., and Schuster, D. I., Tomography in the presence of stray inter-qubit coupling <https://arxiv.org/abs/2103.13611> (2021).
27. Faist, P. & Renner, R. Practical and reliable error bars in quantum tomography. *Phys. Rev. Lett.* **117**, 010404 (2016).
28. Li Ma, S. et al. Coupling-modulation-mediated generation of stable entanglement of superconducting qubits via dissipation. *Europhys. Lett.* **135**, 63001 (2021).
29. Li, Z., Autonomous stabilization with programmable stabilized state <https://doi.org/10.6084/m9.figshare.25249459> (2024).

Acknowledgements

This work was supported by AFOSR Grant No. FA9550-19-1-0399 and ARO Grant No. W911NF-17-S0001. Devices are fabricated in the Pritzker Nanofabrication Facility at the University of Chicago, which receives

support from Soft and Hybrid Nanotechnology Experimental (SHyNE) Resource (NSF ECCS-1542205), a node of the National Science Foundation's National Nanotechnology Coordinated Infrastructure. This work also made use of the shared facilities at the University of Chicago Materials Research Science and Engineering Center, supported by the National Science Foundation under award number DMR-2011854. E.K.'s research was additionally supported by NSF Grant No. PHY-1653820.

Author contributions

These authors contributed equally: Z.L., T.R. Z.L. conceived the experiment. Z.L. designed the device, and T.R. fabricated the device. Z.L. calibrated the experiment and analyzed the data with assistance from T.R. Z.L. performed the simulation with help from T.R. and Y.L. E.K. provided theoretical support and guidance throughout the experiment, and D.I.S. supervised all the aspects of the project. Z.L. and T.R. wrote the manuscript, with input from all the authors.

Competing interests

The authors declare no competing interests.

Additional information

Supplementary information The online version contains supplementary material available at <https://doi.org/10.1038/s41467-024-51262-4>.

Correspondence and requests for materials should be addressed to Ziqian Li.

Peer review information *Nature Communications* thanks Xiu-Hao Deng and the other, anonymous, reviewer(s) for their contribution to the peer review of this work. A peer review file is available.

Reprints and permissions information is available at <http://www.nature.com/reprints>

Publisher's note Springer Nature remains neutral with regard to jurisdictional claims in published maps and institutional affiliations.

Open Access This article is licensed under a Creative Commons Attribution-NonCommercial-NoDerivatives 4.0 International License, which permits any non-commercial use, sharing, distribution and reproduction in any medium or format, as long as you give appropriate credit to the original author(s) and the source, provide a link to the Creative Commons licence, and indicate if you modified the licensed material. You do not have permission under this licence to share adapted material derived from this article or parts of it. The images or other third party material in this article are included in the article's Creative Commons licence, unless indicated otherwise in a credit line to the material. If material is not included in the article's Creative Commons licence and your intended use is not permitted by statutory regulation or exceeds the permitted use, you will need to obtain permission directly from the copyright holder. To view a copy of this licence, visit <http://creativecommons.org/licenses/by-nc-nd/4.0/>.

© The Author(s) 2024